Drug Design, Development and Therapy

Dovepress
open access to scientific and medical research

Open Access Full Text Article

ORIGINAL RESEARCH

Puerarin transport across rat nasal epithelial cells and the influence of compatibility with peoniflorin and menthol

This article was published in the following Dove Press journal:
Drug Design, Development and Therapy
1 September 2017

Lin Zhang
Shou-Ying Du
Yang Lu
Chang Liu
Hui-Chao Wu
Zhi-Hao Tian
Min Wang
Chang Yang

School of Chinese Materia Medica, Beijing University of Chinese Medicine, Chaoyang District, Beijing, People's Republic of China

Abstract: Nose-to-brain transport can provide an excellent pathway for drugs of the central nervous system. Consequently, how to make full use of this pathway in practical applications has become a focus of drug design. However, many aspects affecting drug delivery from the nose to the brain remain unclear. This study aimed to more deeply investigate the transport of puerarin and to explore the mechanism underlying the influence of compatible drugs on puerarin permeability in a primary cell model simulating the nasal mucosa. In this research, based on rat nasal epithelial cells (RNECs) cultured in vitro and cytotoxicity assays, the bidirectional transport of puerarin across RNEC monolayers and the effect of its compatibility with peoniflorin and menthol were analyzed. The apparent permeability coefficient was $<1.5\times10^{-6}$ cm/s, and the efflux ratio of puerarin was <2, indicating that puerarin had poor absorption and that menthol but not peoniflorin significantly improved puerarin transport. Simultaneously, through experiments, such as immunofluorescence staining, transepithelial electrical resistance measurement, rhodamine 123 efflux evaluation, the cell membrane fluorescence recovery after photobleaching test, and ATPase activity determination, the permeability promoting mechanism of menthol was confirmed to be closely related to disruption of the tight junction protein structure, to the P-glycoprotein inhibitory effect, to increased membrane fluidity, and to the promotion of enzyme activity. These results provide reliable data on nasal administration of the studied drugs and lay the foundation for a deeper investigation of the nose–brain pathway and nasal administration.
Keywords: Chinese herbal compound, immunofluorescence, transepithelial electrical resistance, tight junction, P-glycoprotein, membrane fluidity

Introduction

The effects of drugs that play roles in the central nervous system (CNS) and treat cerebral diseases are usually limited by the blood–brain barrier (BBB), the blood–cerebrospinal fluid barrier, and the arachnoid barrier.[1] Among these, BBB has typically been considered the major reason why many CNS-active drugs have difficulty reaching the brain. Over the past several decades, nasal administration has attracted much attention as a unique way to bypass the formidable BBB and deliver CNS-active drugs to the brain, given the direct anatomical and physiological link between the nasal cavity and the CNS.[2] Hence, nasal administration has become a promising alternative to oral or parenteral administration.

Nasal administration systems can provide several types of main transport mechanisms for drugs to arrive in the brain,[3] among which direct nose-to-brain transport (or nerve pathway transport) is the most important. Through this pathway, drugs can be transported through the nasal mucosa to the CNS via extracellular or intracellular

Correspondence: Shou-Ying Du
School of Chinese Materia Medica, Beijing University of Chinese Medicine, No 6, Zhonghuan South Road, Wangjing, Chaoyang District, Beijing 100102, People's Republic of China
Tel +86 10 8473 8615
Fax +86 10 8473 8611
Email dushouying607816@163.com

mechanisms involving trigeminal and olfactory nerves. After reaching the lamina propria, trigeminal nerve endings convey chemosensory information of drugs to the CNS, and drug can pass into the olfactory ensheathing cell channels surrounding the olfactory nerves and then access the cerebrospinal fluid and olfactory bulbs to be distributed throughout the brain.[3] This pathway not only has great potential to bypass the BBB but also avoids the first-pass effect, which improves the bioavailability of a drug. Moreover, drug absorption by the nasal mucosa provides a noninvasive pathway to deliver drugs to the brain and may promote medication adherence in patients. Additionally, other advantages include the fast onset of therapeutic effects and reduced drug side effects.[4]

However, major challenges remain due to the multiple delivery barriers before drugs can effectively reach the brain and show improved treatment efficacy via the nasal administration system.[5] In a sense, nasal epithelial cells could be the first hurdle which limits nasal absorption and thus affect the transmission and bioavailability of the drugs. For hydrophilic drugs that do not easily traverse cell membranes, paracellular transport across nasal epithelial cells is the primary mechanism. However, since tight junctions (TJs) create a firm connection, paracellular transport is highly restricted and only possible for smaller compounds. For lipophilic drugs, transcellular passage can be counteracted by the actions of efflux transporter proteins such as P-glycoprotein (P-gp) as well as multidrug resistance-related proteins that are present on the cell membranes of nasal epithelial cells.[6] Therefore, gaining an insight into the characteristics of drug nasal absorption is essential.

The aim of this study was to further explore the nasal absorption features of puerarin, peoniflorin, and menthol, which are usually used together to treat acute cerebral stroke in Chinese traditional medicine clinics.[7–9] In our previous in vivo study, when puerarin was administered to rats via caudal vein injection, nasal administration, or oral administration and the concentration of puerarin in mice was analyzed in the plasma and brain using reversed-phase high-performance liquid chromatography (HPLC), the result indicated that the bioavailability of puerarin following intranasal administration was significantly higher than that of oral administration, and the ability of puerarin to target the brain via intranasal administration was higher than that with injection and oral administration.[10,11] In addition, we had chosen Calu-3 cells (derived from a human lung adenocarcinoma cell line) to model the nasal mucosa and to preliminarily evaluate the influence of puerarin in combination with peoniflorin and menthol on enhanced cell permeability.[12] The apparent permeability coefficients (P_{app}) of puerarin bidirectional transport were both $<1.5\times10^{-6}$ cm/s, and the efflux ratio (ER) was <1.5, indicating that puerarin alone exhibited poor absorption and that its transport primarily occurred by passive diffusion through the cell monolayer. When puerarin was coadministered with peoniflorin, the P_{app} remained unaltered ($P>0.05$). However, the addition of menthol significantly ($P<0.05$) improved the P_{app} of puerarin in both directions. Moreover, based on immunofluorescence experiments and transepithelial electrical resistance (TEER) measurements, the drug compatibility of puerarin and menthol opened the TJs and weakened the barrier capabilities of epithelial cells, thereby promoting the permeability of puerarin. Although previous studies have evaluated the effects of different administration routes and pharmacokinetic behavior both in vivo and in a surrogate nasal mucosa model, the absorption and transport across real nasal mucosa epithelial cells and the mechanism of this compatibility remain unclear. To better establish an in vivo/in vitro correlation and model drug absorption in actual nasal mucosa, the present study utilized rat nasal epithelial cells (RNECs) as an in vitro cell model to simulate the physiological properties of the nasal mucosa. On this basis, in addition to measuring the influences of drugs on transport behavior, TJs, and TEER, the permeability of these drugs and the mechanism of their mutual compatibility were evaluated from multiple perspectives, including measuring P-gp, membrane fluidity, and Na^+-K^+- and Ca^{2+}-ATPase activities. These experiments provide the basis for further studies of the nose-to-brain pathway.

Materials and methods

Materials

Puerarin (PubChem compound identifier [CID]: 5281807), peoniflorin (PubChem CID: 442534), and menthol (PubChem CID: 16666) were obtained from the National Institute for the Control of Pharmaceutical and Biological Products (Beijing, China). Polyethylene terephthalate (PET) cell culture inserts and 12-well plates (12-mm diameter, 0.4-μm pore size) were purchased from Corning Corporation (Corning, NY, USA). The rabbit anti-zonula occludens 1 (ZO-1) antibody (61-7300) and the mouse anti-claudin-1 antibody (2H10D10) were obtained from Thermo Fisher Scientific (Waltham, MA, USA). Tetramethyl rhodamine isothiocyanate (TRITC, red)-conjugated anti-rabbit IgG antibody was purchased from Beijing Zhongshan Golden Bridge Biotechnology Co, Ltd (Beijing, China). Fluorescein isothiocyanate (FITC, green)-conjugated anti-mouse IgG antibody was purchased from Kangwei Century Biotechnology Co, Ltd (Beijing, China). Acti-stain 488 (green) fluorescent phalloidin was purchased from Cytoskeleton Inc (Denver, CO, USA). 2-(6-(7-nitrobenz-2-oxa-,3-diazol-4-yl)amino) hexanoyl-1-hexadecanoyl-sn-glycero-3-phosphocholine (NBD-C6-HPC) was purchased from Thermo Fisher Scientific. A total protein bicinchoninic acid assay kit, a Na^+-K^+-ATPase assay kit, and a Ca^{2+}-ATPase assay kit were purchased from NanJing JianCheng Bioengineering Institute (NanJing, China). In this study, all experimental protocols were approved by the Review Committee for the Use of Human or Animal Subjects of Beijing University of Chinese Medicine.

Cell culture

RNECs were cultured as previously described, with slight modifications.[13] A male Sprague Dawley rat was killed by an abdominal injection with an overdose of chloral hydrate (Sinopharm Chemical Reagent Co, Ltd, Shanghai, China). The surgical procedure for the rat included removing the skin from the head, cutting along the internasal suture, using surgical scissors and tweezers to remove the nasal bones, and isolating the nasal septum. The nasal mucosal tissue was then quickly stripped from the cartilage of the nasal septum and placed in phosphate-buffered saline (PBS) supplemented with 100 U/mL penicillin and 100 μg/mL streptomycin. The tissue was then transferred into 1.0% protease (type XIV; Sigma, San Francisco, CA, USA) and minced into 2–3 mm^3 pieces. The tissue debris was incubated for 1 hour at 37°C and then removed when the cell suspension was passed through a 40-μm cell strainer. After centrifugation at 1,000 rpm for 3 minutes, the supernatant was discarded, and the dissociated epithelial cells were resuspended in Dulbecco's Modified Eagle's Medium (DMEM; Thermo Fisher Scientific) supplemented with 10% heat-inactivated fetal bovine serum (Thermo Fisher Scientific), 100 U/mL penicillin, and 100 μg/mL streptomycin. The cells were seeded on a plastic dish and incubated at 37°C for 1 hour to eliminate the majority of endothelial cells, fibroblasts, and myoblasts by differential attachment to the bottom of the plastic dish. The suspended epithelial cells that were collected from the plastic dish were inoculated in a culture flask and cultured with DMEM in a humidified atmosphere with 5% CO_2 at 37°C for 24 hours, and the medium was then replaced with serum-free bronchial epithelial cell growth medium (Lonza Group Ltd, Basel, Switzerland). The medium was changed every 2 days until the cells reached ~90% confluence. This study was conducted in accordance with the Declaration of Helsinki and the Guide for Care and Use of Laboratory Animals as adopted and promulgated by the National Institutes of Health (USA).

Cytotoxicity assays

The levels of puerarin, peoniflorin, and menthol that interfered with the growth of RNECs were determined using the 3-(4,5-dimethylthiazol-2-yl)-2,5-diphenyltetrazolium bromide (MTT) dye assay. The cells were seeded at a density of 1×10^5 cells/mL in 96-well flat-bottomed microtiter plates in a total volume of 100 μL of culture medium per well and incubated in a humidified atmosphere with 5% CO_2 at 37°C. After 48 hours, the medium was removed and replaced with fresh medium containing different compounds at various concentrations. After further culture for 24 hours, 20 μL of 5 mg/mL MTT in PBS was added to each well, and the mixtures were incubated at 37°C for 4 hours until purple deposits became visible. The assay measured the amount of MTT reaction products produced by mitochondrial dehydrogenase and assumed that cell viability, corresponding to the reductive activity, was proportional to the production of purple formazan, which was measured spectrophotometrically. After the MTT solutions were discarded, the colored reaction products were completely dissolved by the addition of 20 μL of dimethyl sulfoxide, and the absorbance was measured at 490 nm on a Multiskan GO microplate reader (Thermo Fisher Scientific). The mean absorbance of five measurements for each compound was expressed as a percentage of the absorbance of the untreated control and plotted against the concentration of the compound. The cells were used at passage numbers 2–3.

Transport across RNECs

The integrity and restrictiveness of epithelial cell monolayers in vitro were evaluated by measuring TEER and using microscopy. Cells were plated at a density of 5×10^5 cells/cm^2 onto 0.4-μm pore size, collagen-coated clear PET membranes in 12-mm Transwell chambers and cultured for 3 days under air-interface-feeding conditions. TEER was measured every other day using chopstick electrodes and an epithelial volt–ohm meter instrument (Millipore Corporation, Boston, MA, USA) in association with the replacement of the medium in the basolateral chamber. Cell monolayers were considered to have formed when the TEER value exceeded 500 $\Omega\cdot cm^2$ and when the cells were completely confluent, as observed using microscopy. The formation of these cell monolayers was the basis for further studies.

To determine the permeability of puerarin and the effect of the compatibility of different drugs on penetration, drug transport in the cell monolayers was analyzed. After monolayer formation, the cells were washed three times with Hanks balanced salt solution (HBSS) and equilibrated for 30 minutes at 37°C. The drug solution (0.5 mL) was added to the apical (A) side, and HBSS (1.5 mL) was added to the basolateral (B) side to measure A→B transport. The cells were incubated in a 37°C shaking incubator. Samples (600 μL) were collected from the B side at 30, 60, 90, 120, 150, and 180 minutes. The amount of puerarin that was transported was measured by HPLC using a Hibar C_{18} column (4×200 mm^2, 5 μm). Samples were analyzed using ultraviolet detection (λ=250 nm). The mobile phase consisted of methanol and 1% acetate (37:63, v/v) and was pumped at a flow rate of 1 mL/min, and the injected volume was 20 μL. Under these conditions, the retention time of puerarin was ~6 minutes. B→A transport was evaluated by adding 1.5 mL of the drug solution to the B side and 0.5 mL of HBSS to the A side. Samples (200 μL) were collected from the A side at the same time intervals as above and were measured using the same HPLC method as for the A→B transport measurements. The cells were used at passage numbers 2–3.

Measuring changes in cell TEER

In addition to determining the integrity of the monolayers, cell TEER was measured to investigate changes in TJ function in RNECs. After the cells formed monolayers, 0.5 mL of drug solution was added to the A side, and 1.5 mL of HBSS was added to the B side to simulate A→B transport. B→A transport was similarly evaluated by adding 1.5 mL of drug solution to the B side and 0.5 mL of HBSS to the A side. The TEER values of the untreated cells and of cells treated with puerarin, peoniflorin, and (or) menthol were determined at 30, 60, 90, 120, 150, and 180 minutes. The measured TEER value before the experiment was set as 100%, and all other values were calculated relative to this value. Then, the relative TEER value at each time point was compared with the control group value and statistically analyzed.

Immunofluorescence microscopy

For immunocytochemistry research on TJ proteins, cells were grown at a density of 5×10^5 cells/cm^2 on PET membranes in Transwell chambers until the formation of monolayers, after which the cells were loaded with media containing different compounds for 3 hours at 37°C. Then, the cells were first fixed with cold 4% paraformaldehyde for 30 minutes. After a PBS rinse, the cells were next blocked for 1 hour with goat serum, and some samples were then incubated overnight with polyclonal anti-ZO-1 (1:100) or monoclonal anti-claudin-1 (1:100) primary antibodies at 4°C. After three washes with PBS, the cells were incubated with the secondary antibodies, TRITC (red)-conjugated anti-rabbit IgG or FITC (green)-conjugated anti-mouse IgG. Some cells were only stained with acti-stain 488 (green) fluorescent phalloidin (1:150) at room temperature for 30 minutes. DAPI (Solarbio, Beijing Solarbio Science and Technology Co, Ltd, Beijing, China) was used to counterstain the cell nuclei. The membranes were carefully excised from the Transwell inserts, mounted on glass slides with 80% glycerol, and covered with 15-mm coated cover glass. The morphology and fluorescence of TJ proteins were visualized on an inverted fluorescence microscope equipped with an appropriate filter (Olympus, Tokyo, Japan) and a laser scanning confocal microscope, and images were obtained using the analysis software. The settings for image collection were identical, and the average optical density (AOD) of the images was calculated using ImageJ software. The cells were used at passage numbers 2–3.

Flow cytometric detection of cell surface P-gp

The intracellular accumulation of the fluorescent dye rhodamine 123 (Rho 123) is frequently used in functional assays of P-gp.[14] RNEC monolayers in Transwell chambers were loaded for 3 hours at 37°C with media containing different compounds. Verapamil (Beijing LeBo Biotech Company, Beijing, China), a known P-gp inhibitor, was used as a positive control.[14] Cells were then incubated for 1 hour with Rho 123 (5 μg/mL) at 37°C. After incubation, the cells were washed twice with PBS and then harvested from the Transwell inserts by trypsinization. Cell fluorescence was measured on a flow cytometer (FCM; Becton Dickinson, Franklin Lakes, NJ, USA). Each measurement counted 10,000 events. Nonviable cells were gated out of the analysis on the basis of side scatter. The P1 FITC-A mean was the fluorescence intensity value of the 10,000 events of each group, and the P2 percentage was the proportion of the greater fluorescence intensity.

Na^+-K^+- and Ca^{2+}-ATPase activity assays

Because the ATP enzyme activity value computation was based on the total protein content, the total protein assay kit was adopted firstly. The total protein content of the RNECs at a density of 1×10^6 cells/cm^2 was 0.4696±0.0010 mg/mL. Then, ATPase kits (Na^+, K^+, and Ca^{2+}-ATP) were employed to detect the energy metabolism changes of each group of cells at a density of 1×10^6 cells/cm^2, after RNECs monolayers in Transwell chambers were loaded for 3 hours at 37°C with media containing different compounds. The ATP enzyme activity values were calculated according to the manufacturer's instructions for each kit and using improved inorganic phosphate microanalyses.

Fluorescence recovery after photobleaching (FRAP) detection of membrane fluidity

FRAP is sensitive to the presence of barriers to diffusion that may be present within the membrane resulting in domain formation. In FRAP, a small region of interest is photobleached by a laser pulse and then the diffusion coefficients can be determined by measuring the time course of fluorescence recovery, which reflects membrane fluidity. For the FRAP experiment on membrane fluidity, cells were grown at a density of 2×10^5 cells/cm^2 in glass bottom dishes until cell fusion reached $>80\%$. Then, the cells were loaded with media containing different compounds for 3 hours at 37°C. RNEC membrane phospholipids were fluorescently labeled with NBD-C6-HPC for 30 minutes, and after three washes with PBS, membrane fluidity was measured using confocal scanning laser microscopy. The fluorescence recovery rates (R) were calculated according to the formulation.[15]

Data analysis and statistics

Cell viability (percentage) in the MTT assay was calculated using the following equation

$$\text{Viability}(\%)=\frac{A_{\text{sample}}-A_{\text{blank}}}{A_{\text{control}}-A_{\text{blank}}}\times 100 \quad (1)$$

where A is the absorbance value.

The apparent permeability coefficients (P_{app}) for puerarin were calculated according to the following equation

$$P_{\text{app}}=\frac{dQ/dt}{CS} \quad (2)$$

where dQ/dt is the apparent appearance rate of puerarin on the receiver side, which was calculated using a linear regression of the amount of puerarin in the receiver chamber at different time points; C is the puerarin concentration in the donor chamber; and S is the surface area of the PET membrane of the Transwell chamber.

ER was calculated according to the following equation

$$\text{ER}=\frac{P_{\text{app}}(\text{B}\rightarrow\text{A})}{P_{\text{app}}(\text{A}\rightarrow\text{B})} \quad (3)$$

The immunofluorescence images were semiquantitatively analyzed using ImageJ software according to the following equation

$$\text{AOD}=\frac{\text{IntDen}}{\text{Area}} \quad (4)$$

where IntDen is the integrated optical density in the image, and Area is the region of fluorescence in the image.

The AOD percentage corresponding to the TJ protein was calculated using the following equation

$$\text{Relative AOD}(\%)=\frac{\text{AOD}_{\text{sample}}}{\text{AOD}_{\text{control}}}\times 100 \quad (5)$$

The ATP enzyme activity values were calculated using the following equation ATP enzyme activity values (μmolPi/mgprot/hour)

$$=\frac{A_{\text{sample}}-A_{\text{control}}}{A_{\text{standard}}-A_{\text{blank}}}\times \text{lankardour}\div 0.4696 \quad (6)$$

where A is the absorbance value.

The fluorescence recovery rates (R) for the membrane fluidity were calculated using the following equation

$$\text{R}(\%)=\frac{\text{F}_2-\text{F}_0}{\text{F}_1-\text{F}_0}\times 100 \quad (7)$$

where F_0 is the fluorescence intensity at the time of photobleaching, F_1 is the fluorescence intensity before photobleaching, and F_2 is the fluorescence intensity after recovery.

Each set of results shown is representative of three separate experiments. The results are given as the mean ± standard deviation. The data were analyzed by one-way analysis of variance, followed by Dunnett's test to compare differences among multiple groups and the control group (using SPSS 17.0 statistical software; SPSS Inc, Chicago, IL, USA). Significance was set at $P<0.05$.

Results

Cytotoxicity of the compounds in RNECs

The cytotoxicity results are shown in Figure 1. The puerarin, peoniflorin, and menthol groups showed no cytotoxicity in RNECs in the respective concentration ranges of 0–300, 0–200, and 0–50 μg/mL (Figure 1A–C). The puerarin combined with peoniflorin group (puerarin:peoniflorin, 1:0.4, w/w)

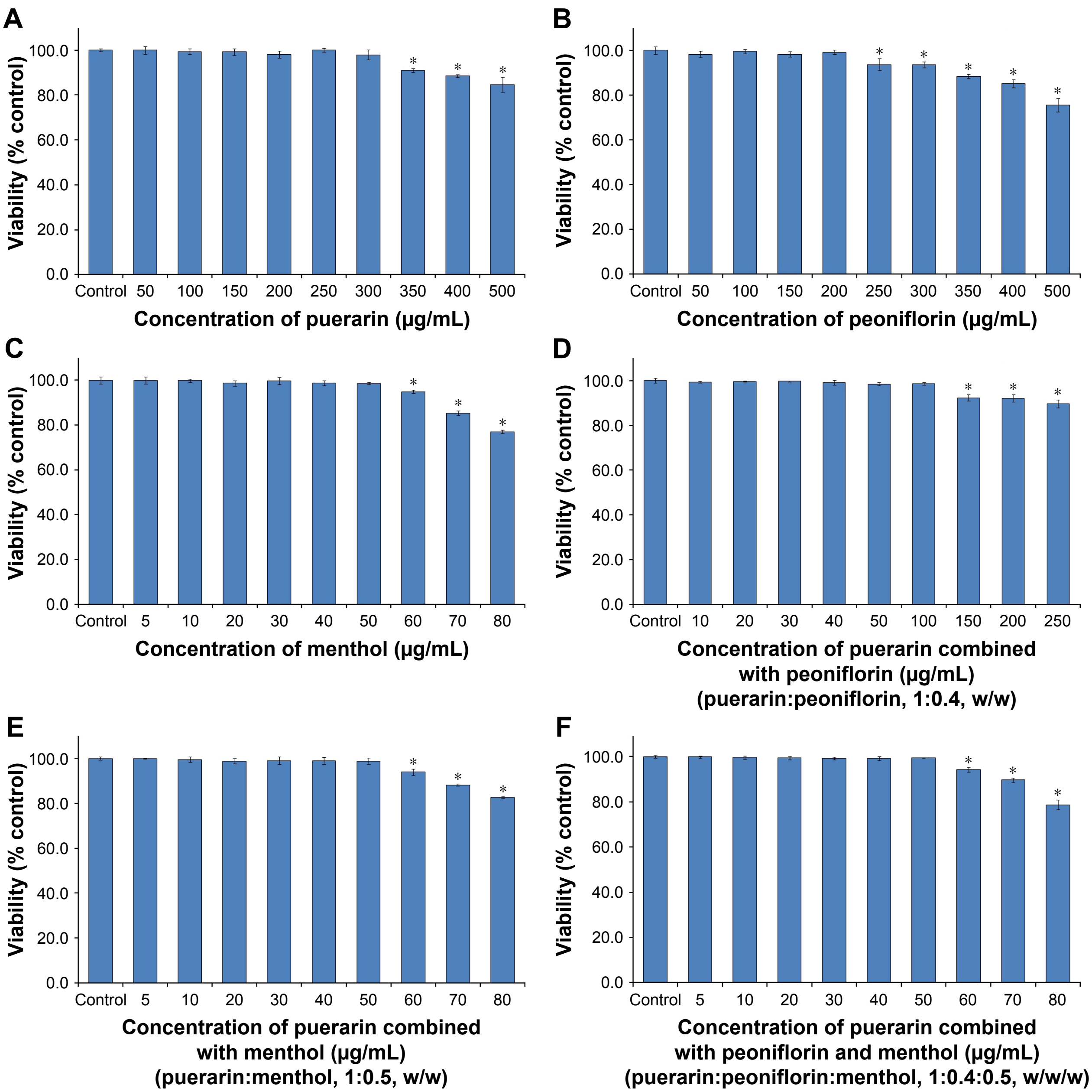

Figure 1 Cytotoxicity of puerarin, peoniflorin, menthol, and their combinations, as determined by the MTT assay in RNECs.
Notes: Cytotoxicity of (**A**) puerarin, (**B**) peoniflorin, (**C**) menthol, (**D**) puerarin combined with peoniflorin, (**E**) puerarin combined with menthol, (**F**) puerarin combined with peoniflorin and menthol. Data are expressed as the mean ± SD (n=5). *$P<0.05$ compared with the control group.
Abbreviations: MTT, 3-(4,5-dimethylthiazol-2-yl)-2,5-diphenyltetrazolium bromide; RNECs, rat nasal epithelial cells; SD, standard deviation.

showed no cytotoxicity in the concentration range of 0–100 μg/mL, which is graphed in terms of the peoniflorin concentration (Figure 1D). The puerarin combined with menthol group (puerarin:menthol, 1:0.5, w/w) showed no cytotoxicity in the concentration range of 0–50 μg/mL, which is graphed in terms of the menthol concentration (Figure 1E). The puerarin combined with peoniflorin and menthol group (puerarin:peoniflorin:menthol, 1:0.4:0.5, w/w/w) showed no cytotoxicity in the concentration range of 0–50 μg/mL, which is graphed in terms of the menthol concentration (Figure 1F).

Puerarin transport across RNECs

Puerarin transport across RNECs was studied at three concentrations: 25, 50, and 100 μg/mL. The results are summarized in Table 1. The transepithelial flux of puerarin was investigated in both transport directions (A→B and B→A) to determine whether its transport was polarized. The P_{app} (A→B) of puerarin was between 1.272×10^{-6} and 1.313×10^{-6} cm/s. The P_{app} (B→A) of puerarin was between 1.351×10^{-6} and 1.411×10^{-6} cm/s. The flux of puerarin from the A side to the B side showed no significant difference compared with that from the B

Table 1 Transport of increasing concentrations of puerarin across RNEC monolayers

Condition (μg/mL)	P_{app} (A→B) (×10^{-6} cm/s)	P_{app} (B→A) (×10^{-6} cm/s)	ER (B→A/A→B)
25	1.272±0.293	1.376±0.087	1.083±0.085
50	1.309±0.083	1.351±0.026	1.035±0.075
100	1.313±0.035	1.411±0.020	1.075±0.024

Note: Values are the mean ± SD (n=3).
Abbreviations: A, apical side; B, basolateral side; ER, efflux ratio; P_{app}, apparent permeability coefficient; RNEC, rat nasal epithelial cell; SD, standard deviation.

side to the A side ($P>0.05$). The ER for each puerarin concentration was ~1.

The effects of different drug interactions on puerarin transport in RNECs are presented in Tables 2 and 3. The effects of peoniflorin were studied at 10, 20, and 40 μg/mL in the presence of 50 μg/mL puerarin, and the P_{app} (A→B and B→A) values did not differ significantly from those of the control group ($P>0.05$). The effects of menthol were studied at 12.5, 25, and 50 μg/mL in the presence of 50 μg/mL puerarin. Menthol significantly increased the puerarin flux in both directions in a concentration-dependent manner (25 and 50 μg/mL, $P<0.05$). The effects of both peoniflorin and menthol were studied at the aforementioned concentrations in the presence of 50 μg/mL puerarin. In the presence of 10 μg/mL peoniflorin and 12.5 μg/mL menthol, the B→A fluxes of puerarin were significantly increased ($P<0.05$). Peoniflorin and menthol together (20 μg/mL peoniflorin and 25 μg/mL menthol or 40 μg/mL peoniflorin and 50 μg/mL menthol) also significantly increased the puerarin fluxes in both directions in a concentration-dependent manner ($P<0.05$).

TEER changes in RNECs

The results are shown in Figure 2. In RNECs, the puerarin group (25, 50, or 100 μg/mL puerarin) and the puerarin and peoniflorin group (50 μg/mL puerarin combined with 10, 20, or 40 μg/mL peoniflorin) showed TEER change trends that were analogous to those in the control group for the A→B and B→A transport processes throughout the detection. From 60 minutes, the TEER of the puerarin and menthol group (50 μg/mL puerarin combined with 12.5, 25, or 50 μg/mL menthol) and the puerarin, peoniflorin, and menthol group (50 μg/mL puerarin combined with 10, 20, or 40 μg/mL peoniflorin and 12.5, 25, or 50 μg/mL menthol) decreased and showed a significant difference from the control group ($P<0.05$). The decreased TEER, which resulted from compatibility with menthol, showed a concentration-dependent behavior in the studied range.

Table 2 Effects of peoniflorin and menthol on the transport of puerarin in RNECs

Condition (μg/mL)	P_{app} (A→B) (×10^{-6} cm/s)	P_{app} (B→A) (×10^{-6} cm/s)	ER (B→A/A→B)
Pu (50) (control)	1.309±0.083	1.351±0.026	1.035±0.075
+ Pa (10)	1.339±0.102	1.421±0.096	1.063±0.078
+ Pa (20)	1.311±0.062	1.343±0.059	1.025±0.050
+ Pa (30)	1.307±0.358	1.393±0.023	1.066±0.043
+ Me (12.5)	1.381±0.053	1.393±0.053	1.011±0.076
+ Me (25)	1.936±0.126*	1.899±0.140*	0.985±0.114
+ Me (50)	2.153±0.220*	2.201±0.071*	1.030±0.118
+ Pa (10) + Me (12.5)	1.319±0.034	1.560±0.081*	1.182±0.035
+ Pa (20) + Me (25)	1.876±0.174*	1.825±0.085*	0.978±0.095
+ Pa (40) + Me (50)	2.007±0.100*	2.200±0.141*	1.095±0.034

Notes: Values are the mean ± SD (n=3). Differs from Pu (50 μg/mL): *$P<0.05$.
Abbreviations: A, apical side; B, basolateral side; ER, efflux ratio; Me, menthol; P_{app}, apparent permeability coefficient; Pa, peoniflorin; Pu, puerarin; RNECs, rat nasal epithelial cells; SD, standard deviation.

Table 3 Effects of verapamil, puerarin, peoniflorin, and menthol on Rho 123 efflux from RNECs

Group	P1 FITC-A mean	P2 %parent
Control	15.667±0.577	–
Rho 123	8,568.667±212.731	63.133±2.854
Verapamil + Rho 123	12,557.000±198.325*	83.167±2.120*
Puerarin + Rho 123	9,844.333±80.476*	71.933±1.750*
Peoniflorin + Rho 123	9,354.000±158.237*	68.533±1.877*
Menthol + Rho 123	10,765.667±318.858*	75.900±1.539*

Notes: Values are the mean ± SD (n=3). Differs from Rho 123: *$P<0.05$.
Abbreviations: FITC, fluorescein isothiocyanate; Rho 123, rhodamine 123; RNECs, rat nasal epithelial cells; SD, standard deviation.

Effect of compounds on TJ proteins

The immunohistochemistry results are shown in Figure 3, and the results calculated from the AOD values are shown in Figure 4. Three types of TJ proteins were clearly observed in RNECs; ZO-1 was stained red, claudin-1 and F-actin were stained green, and the nucleus stained blue. After treatment with puerarin (50 μg/mL) or peoniflorin (20 μg/mL), the immunostaining for the three types of TJ proteins was similar to the control group. However, when the cells were incubated with menthol (25 μg/mL), the fluorescence intensity was weaker than that of the control group. Moreover, as calculated by ImageJ and analyzed by SPSS 17.0, the control, puerarin, and peoniflorin groups had approximately similar AOD values, whereas the difference compared to the menthol group and the control group was statistically significant ($P<0.05$).

Effect of compounds on the surface expression of P-gp in RNECs

The results of P-gp expression measured by FCM are shown in Figure 5. When compared with the no-treatment group (Figure 5A), there was a greater intracellular fluorescence

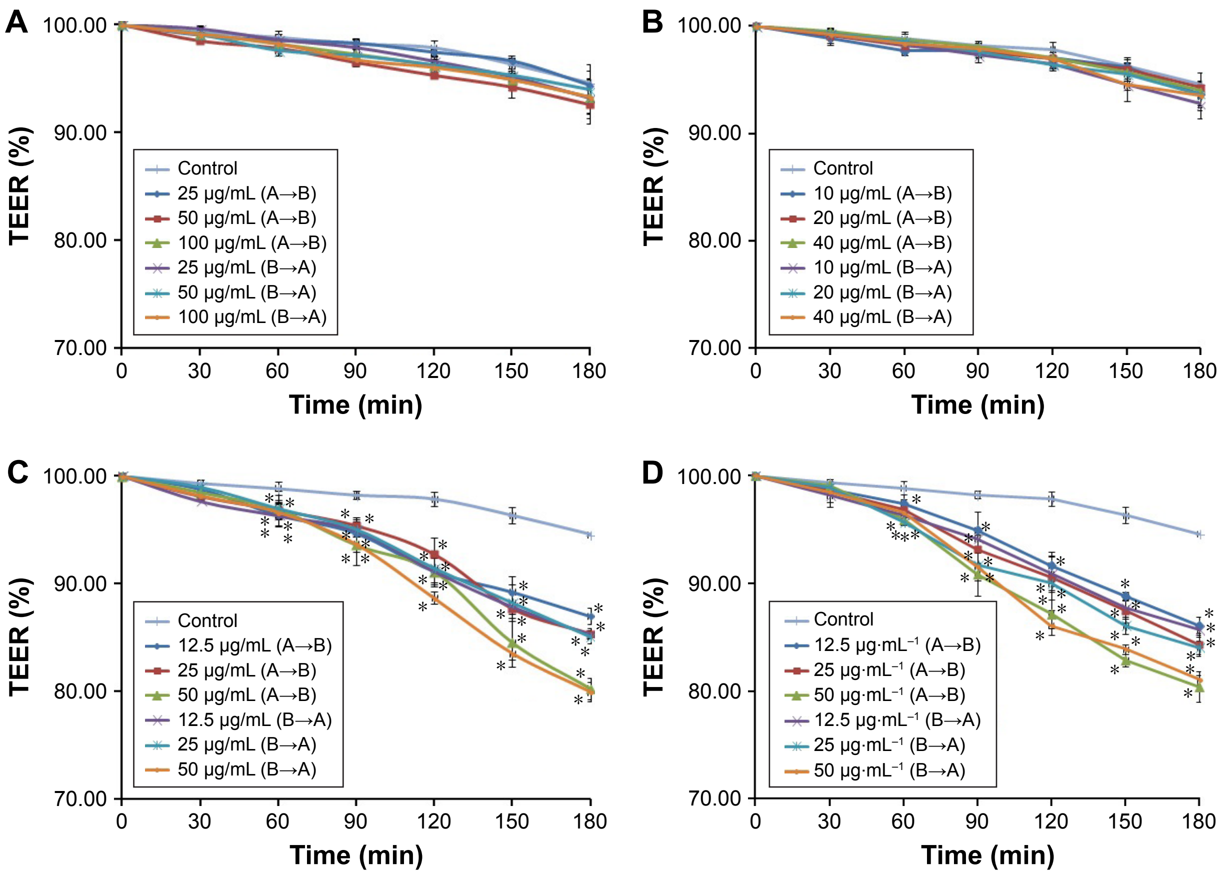

Figure 2 Trend in TEER changes in the A→B and B→A transport of RNECs after treatment with puerarin alone or in combination with different concentrations of peoniflorin or menthol.

Notes: (**A**) Exposure to different concentrations of puerarin resulted in no significant change in TEER compared with the control group. (**B**) Exposure to a specific concentration of puerarin combined with different concentrations of peoniflorin showed no significant changes in TEER. (**C**) Exposure to a specific concentration of puerarin combined with different concentrations of menthol resulted in a significant decrease in TEER compared with the control group. (**D**) Exposure to a specific concentration of puerarin combined with different concentrations of peoniflorin and menthol resulted in a significant decrease in TEER compared with the control group. The TEER value at each time point is represented by the mean ± SD (n=3). Significant difference in TEER from the untreated cells: *$P<0.05$.

Abbreviations: A, apical side; B, basolateral side; RNECs, rat nasal epithelial cells; SD, standard deviation; TEER, transepithelial electrical resistance.

intensity peak after adding Rho 123 (Figure 5B), which suggested that Rho 123 could enter RNECs and the expression of P-gp on the membrane of RNECs seemed to be weak. However, the peak area caused by Rho 123 was significantly increased by incubating with verapamil (Figure 5C), proving a proper surface expression of P-gp in RNECs and indicating the depolarization function of verapamil. After RNECs were incubated with puerarin (50 μg/mL; Figure 5D), peoniflorin (20 μg/mL; Figure 5E), and menthol (25 μg/mL; Figure 5F), the influx of Rho 123 into the cells was also increased. The intracellular fluorescence intensity of Rho 123 was significantly increased following treatment with the compounds, indicating that puerarin, peoniflorin, and menthol were P-gp substrates that prevented the export of the dye from the cells (Table 3). The order of the inhibitory efficiency (average of the P1 FITC-A mean and the P2 percentage) was verapamil > menthol > puerarin > peoniflorin (Table 3).

Changes in Na^+-K^+- and Ca^{2+}-ATPase activity

The results of the Na^+-K^+- and Ca^{2+}-ATPase activity assays are shown in Table 4. Compared with the control group (treated with 50 μg/mL puerarin), Na^+-K^+-ATPase activity did not significantly change in the compatibility group. However, the compatibility group had an impact on Ca^{2+}-ATPase activity. When the concentration of menthol was above 25 μg/mL, whether alone or in combination with peoniflorin, Ca^{2+}-ATPase activity was significantly promoted in RNECs ($P<0.05$).

Effect of the compounds on membrane fluidity

The results of the membrane fluidity test are also shown in Table 4. From the data, peoniflorin combined with puerarin alone had no significant effect. When menthol was added

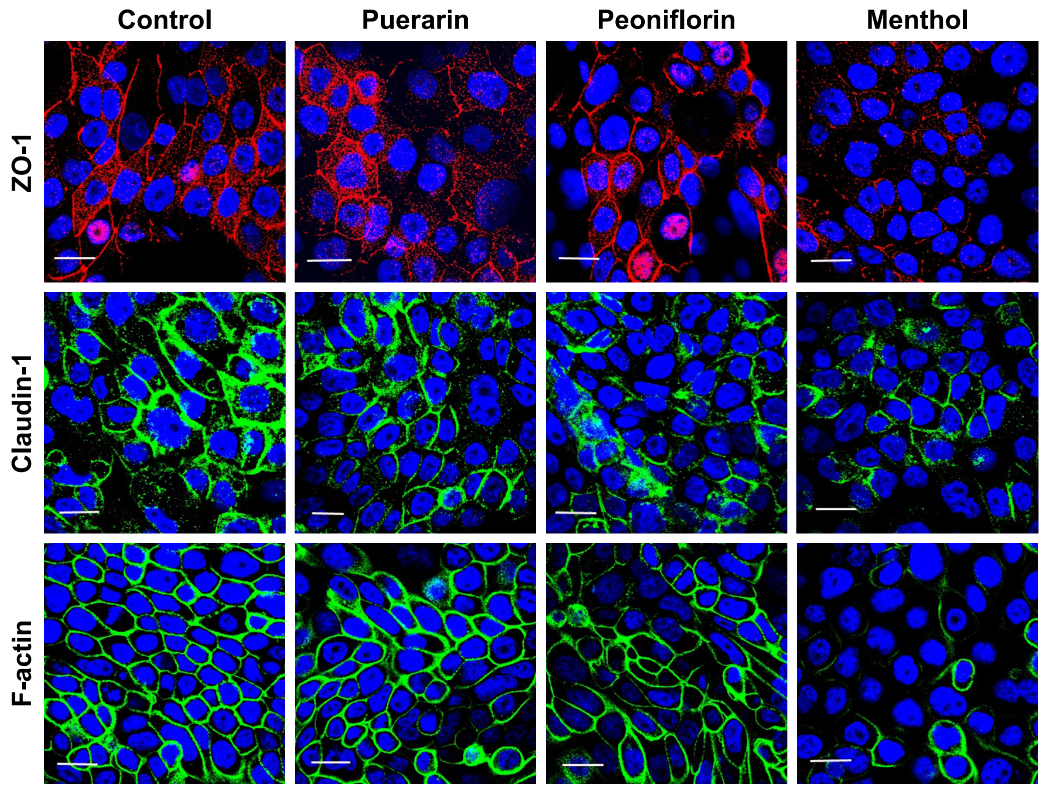

Figure 3 Effects of puerarin, peoniflorin, and menthol on TJ proteins in RNECs.
Notes: Immunocytochemistry showed no differences in staining for the three types of TJ proteins in RNECs treated with puerarin or peoniflorin compared with the control group, whereas staining for the three TJ proteins was significantly decreased after menthol treatment. The scale bar corresponds to 15 µm. Magnification ×600.
Abbreviations: RNECs, rat nasal epithelial cells; TJ, tight junction; ZO-1, zonula occludens 1.

in combination at concentrations over 25 µg/mL, the membrane fluorescence of RNECs showed faster recovery after photobleaching, and the average fluorescence recovery rate was significantly increased ($P<0.05$).

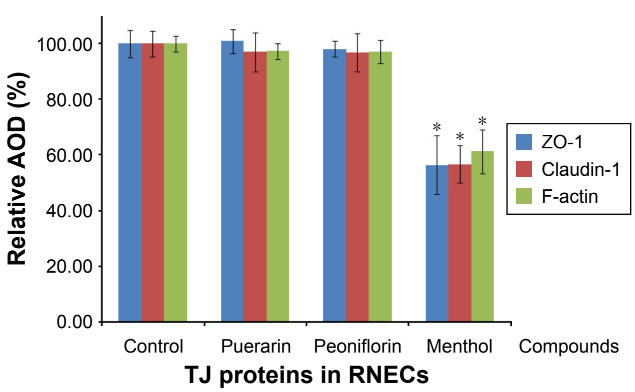

Figure 4 Changes in the relative AOD of ZO-1, claudin-1, and F-actin in RNECs after treatment with different compounds.
Notes: The relative AOD values for the TJ proteins did not significantly differ after treatment with puerarin or peoniflorin compared with the control group ($P>0.05$), whereas the values of the menthol group decreased significantly ($P<0.05$). Data are shown as the mean ± SD (n=3). *$P<0.05$ compared with the value in the control group.
Abbreviations: AOD, average optical density; RNECs, rat nasal epithelial cells; SD, standard deviation; TJ, tight junction; ZO-1, zonula occludens 1.

Discussion

In our prophase research, we evaluated the absorption and transport of the drugs puerarin, peoniflorin, and menthol in Calu-3 cells; however, we wanted to investigate their "true" properties in a primary nasal epithelial model, which more close mimics normal physiological conditions and could bridge the gap to the previous results of animal research in vivo. Rats are most often used as a preclinical animal model in direct nose-to-brain drug delivery studies,[2,16–18] which is in agreement with our previous research in vivo. Therefore, using a primary culture technique, nasal epithelial cells were collected from the rat nasal septum and then cultured in a suitable medium.

In the present study, transport experiments showed similar P_{app} values for the different concentrations of puerarin (both A→B and B→A), and indicated that the transport velocity increased with increasing concentrations of puerarin. Together with the unpolarized transport findings, these results confirmed that puerarin crosses the RNEC monolayer largely via passive diffusion. Puerarin has been reported to be a P-gp substrate,[19] and the FCM experiments described herein demonstrate that RNECs express P-gp to some extent,

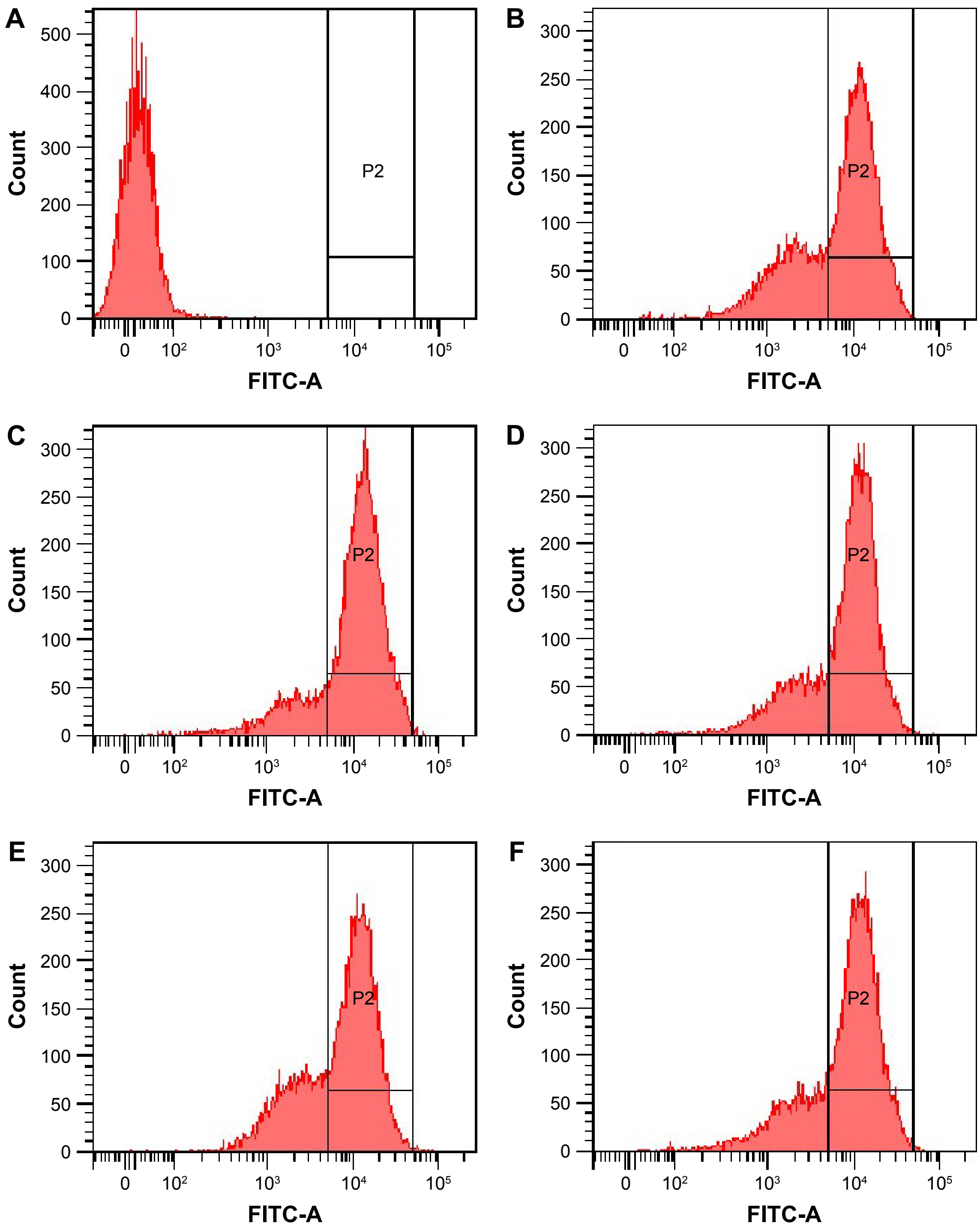

Figure 5 Flow cytometry histograms of Rho 123 accumulation in RNECs.
Notes: (**A**) Cells received no further treatment. The cells were treated with (**B**) only Rho 123, (**C**) verapamil (5 μg/mL) and Rho 123, (**D**) puerarin (50 μg/mL) and Rho 123, (**E**) peoniflorin (20 μg/mL) and Rho 123, (**F**) menthol (25 μg/mL) and Rho 123. P2 percentage was the proportion of the greater fluorescence intensity.
Abbreviations: FITC, fluorescein isothiocyanate; Rho 123, rhodamine 123; RNECs, rat nasal epithelial cells.

but active extrusion via P-gp was not observed. The reason for this phenomenon is that puerarin transport across the monolayer is a complex process. Interestingly, when the compounds were administered at a lower concentration, the effects of P-gp were more significant, whereas at higher concentrations, the simple diffusion rates of many of the P-gp substrates were much greater compared with efflux. Therefore, in the dose range tested in the present study, the transport experiments only characterized the passive diffusion of puerarin. In addition, the drug compatibility assays

Table 4 Influences of puerarin combined with peoniflorin or menthol on ATP enzyme activity and membrane fluidity in RNECs

Condition (μg/mL)	ATP enzyme activity values (μmolPi/mgprot/hour)		R (%)
	Na^+-K^+-ATPase	Ca^{2+}-ATPase	
Control (Pu 50)	0.513±0.006	0.5269±0.005	46.974±1.622
Pu 50 + Pa 10	0.511±0.007	0.524±0.005	46.215±1.503
Pu 50 + Pa 20	0.510±0.008	0.526±0.010	46.334±1.484
Pu 50 + Pa 40	0.506±0.006	0.530±0.011	46.702±1.726
Pu 50 + Me 12.5	0.513±0.004	0.523±0.005	48.563±1.585
Pu 50 + Me 25	0.510±0.008	0.572±0.007*	57.446±2.840*
Pu 50 + Me 50	0.510±0.006	0.602±0.004*	77.927±3.575*
Pu 50 + Pa 10 + Me 12.5	0.508±0.002	0.527±0.002	48.807±1.652
Pu 50 + Pa 20 + Me 25	0.509±0.009	0.593±0.010*	58.810±3.642*
Pu 50 + Pa 40 + Me 50	0.508±0.004	0.621±0.005*	77.343±2.419*

Notes: Values are the mean ± SD (n=3). Differs from the control group: $^*P<0.05$.
Abbreviations: Me, menthol; Pa, peoniflorin; Pu, puerarin; RNECs, rat nasal epithelial cells; SD, standard deviation.

showed that menthol significantly facilitated the transport and improved the permeability of puerarin, whereas peoniflorin had no effect. These results are similar to those identified in the Calu-3 cell model.

To determine the transport mechanism of puerarin in RNECs, as well as the role of drug compatibility in improving permeability, we studied the influence of the various drugs on the related transport indices. For paracellular transport, the physiological function of TJs and changes in the TEER value were employed as the indicators. TJs act as a semipermeable barrier (or gate) to paracellular transport and consist of a series of integral membrane proteins, including claudins, occludin, several peripheral membrane proteins such as ZO-1, ZO-2, ZO-3, cingulin, symplekin, and actin, and an atypical protein kinase C-interacting protein.[20–22] In the present study, representative TJ proteins, including ZO-1, claudin-1, and F-actin, were selected to assay the influence of each compound on TJ structure. Based on the immunofluorescence results and the semiquantitative analysis of the calculated AOD of these chosen TJ proteins, we speculated that menthol disrupted the configuration and integrity of TJs. It is important to note that due to the semiquantitative analysis, the method of evaluating the TJ proteins expression is flawed in a way, but it could be enough to reflect the real state. In addition, TEER, which is closely related to TJs and is affected by cell–substrate contact, can be used to characterize paracellular resistance. In the process of passive transport, paracellular transport of ions and substrates can pass through both the strand breaks of TJs and the pore structures that contacting lateral TJs create. TEER measurements are subject to the flow and type of ions present traveling across the epithelial layer. Therefore, when paracellular transport is enhanced, the TEER value is low. In our research, the TEER value gradually decreased when menthol was added to the cells, whereas the TEER values of the other groups were relatively stable during the test period. Thus, these results confirmed that menthol can weaken the barrier of the nasal mucosa and enhance paracellular transport. The mechanism underlying the effects of menthol may be based on the phosphorylation of TJ components, the activation of protein kinases, the depletion of calcium, or variations in the activity of intrinsic membrane proteins.[23–25] In particular, in terms of the depletion of calcium, the ATPase experiment showed that menthol has the ability to significantly promote Ca^{2+}-ATPase activity in RNECs, which provides a convincing explanation and strong support for the influence of menthol on TJ proteins.

The activity of P-gp is directly related to transmembrane transport. The retention of Rho 123 by cells is considered a test for P-gp function.[26] Our study showed that puerarin, peoniflorin, and menthol all inhibited the function of P-gp and increased the influx of Rho 123. The P-gp inhibitory effect of these drugs may be because they are P-gp substrates[14,19,27] that can competitively bind the P-gp receptor. Therefore, in theory, when combined with peoniflorin or menthol, the transmembrane transport of puerarin in the nasal mucosa should improve, although by only a small amount. P-gp-mediated transport usually involves the energy metabolism of Na^+-K^+-ATPase; however, the Na^+-K^+-ATPase activity in RNECs was very similar among the various drug groups, demonstrating that the effects of puerarin, peoniflorin, and menthol on P-gp were limited. From these results, the conclusion that puerarin crosses the RNEC monolayer largely via passive diffusion was also further confirmed.

Membrane fluidity has been shown to affect numerous membrane functions, including passive permeability properties, the accessibility of receptors, the activity of enzymes, and transport systems.[28] Based on the average fluorescence recovery rate test results, menthol probably increased the membrane fluidity of RNECs, which contributes to improve the permeability of puerarin. Major determinants of membrane fluidity can be classified within two categories: extrinsic determinants (environmental factors) and intrinsic determinants (such as protein and phospholipid contents and compositions), but these factors usually have polygonal and complex relationships. From this experiment, the results can only infer that menthol might have an effect on the membrane fluidity of RNECs, but the exact mechanism is yet to be determined.

Conclusion

In conclusion, following cytotoxicity assays, the bidirectional transport of puerarin across RNEC monolayers, as well as the effect of compatibility with peoniflorin and menthol, was analyzed. The results showed that puerarin is poorly absorbed and that the transport of puerarin mainly occurs via paracellular passive diffusion; however, the permeability of puerarin can be increased by menthol, as well as in Calu-3 cells. Moreover, the complicated transport of puerarin across the nasal mucosa involved both paracellular and transmembrane transport but mainly occurred via passive diffusion through paracellular transport. Menthol, a compatible permeation enhancer, could disrupt TJ structure by inhibiting the expression of TJ proteins, including ZO-1, claudin-1, and F-actin, weaken the barrier function of TJs, decrease the TEER value, promote Ca^{2+}-ATPase activity, and improve membrane fluidity to enhance paracellular transport across the nasal epithelium. The results in this study were consistent with prior work in vivo and in vitro. These studies were conducted to better understand the fundamental pharmacological properties and drug interactions of puerarin and to lay the foundation for a deeper investigation of nose–brain pathways and nasal administration. However, transport from the nose to the brain is a complicated and comprehensive process, and more research is required. Meanwhile, it is very important to realize that major differences exist in nasal features between animals and humans, particularly with regard to the predictive value of preclinical animal models for human applications.

Acknowledgments

The authors thank Jing Han of the Beijing University of Chinese Medicine for her suggestions on the immunofluorescence studies and Zhen-Zhen Chen of the Capital Medical University for his helpful advice on the cell culture experiments. This project was supported by the National Natural Science Foundation of China (no 81473363) and the Self-Topic Fund of Beijing University of Chinese Medicine (no 2015-JYB-XS053).

Disclosure

The authors report no conflicts of interest in this work.

References

1. Abbott NJ, Patabendige AA, Dolman DE, Yusof SR, Begley DJ. Structure and function of the blood–brain barrier. *Neurobiol Dis*. 2010; 37(1):13–25.
2. Ruigrok MJ, de Lange EC. Emerging insights for translational pharmacokinetic and pharmacokinetic-pharmacodynamic studies: towards prediction of nose-to-brain transport in humans. *AAPS J*. 2015; 17(3):493–505.
3. Dhuria SV, Hanson LR, Frey WH. Intranasal delivery to the central nervous system: mechanisms and experimental considerations. *J Pharm Sci*. 2010;99(4):1654–1673.
4. Yan L, Wang H, Jiang Y, et al. Cell-penetrating peptide-modified PLGA nanoparticles for enhanced nose-to-brain macromolecular delivery. *Macromol Res*. 2013;21(4):435–441.
5. Costantino HR, Illum L, Brandt G, Johnson PH, Quay SC. Intranasal delivery: physicochemical and therapeutic aspects. *Int J Pharm*. 2007;337(1–2):1–24.
6. Fortuna A, Alves G, Serralheiro A, Sousa J, Falcão A. Intranasal delivery of systemic-acting drugs: small-molecules and biomacromolecules. *Eur J Pharm Biopharm*. 2014;88(1):8–27.
7. Zengxiang Q. [Pharmacological action and application of Gegentang]. *Chin Trad Patent Mater*. 1996;18(4):43–44. Chinese.
8. Jian Z, Min Z. [Gegentang treated 36 post-stroke depression patients]. *J Jilin Univ Med Ed*. 2009;3(9):569. Chinese.
9. Jiai Y, Yue D, Shupang A. [Pharmacological and clinical researches of Gegentang]. *Chin Arch Trad Chin Med*. 2007;25(6):1275–1278. Chinese.
10. Xiaolan C, Shouying D, Yang L, et al. [Study on pharmacokinetics of puerarin in rats following different methods of administration of Tongqiao Sanyu prescription]. *Zhongguo Zhong Yao Za Zhi*. 2011; 36(17):2347–2349. Chinese.
11. Chen XL, Du SY, Lu Y, et al. [Study on pharmacokinetics of puerarin in rats by following different methods of administration of puerariae extract]. *China J Trad Chin Med Pharm*. 2011;27(10):2408–2411. Chinese.
12. Zhang L, Du SY, Lu Y, et al. Puerarin transport across a Calu-3 cell monolayer – an in vitro model of nasal mucosa permeability and the influence of paeoniflorin and menthol. *Drug Des Devel Ther*. 2016; 10:2227–2237.
13. Vernon ES, Julia TA. Isolation and long-term culture of rat, rabbit, and human nasal turbinate epithelial cells. *In Vitro Cell Dev Biol*. 1985; 21(12):681–687.
14. Eid SY, El-Readi MZ, Eldin EE, Fatani SH, Wink M. Influence of combinations of digitonin with selected phenolics, terpenoids, and alkaloids on the expression and activity of P-glycoprotein in leukaemia and colon cancer cells. *Phytomedicine*. 2013;21(1):47–61.
15. Yguerabide J, Schmidt JA, Yguerabide EE. Lateral mobility in membranes as detected by fluorescence recovery after photobleaching. *Biophys J*. 1982;40(1):69–75.
16. Fening SW, Jollick JA, Huang YT. Calu-3/A-549 mixed cells as a replacement for primary rhesus monkey kidney cells for virus detection. *J Clin Virol*. 2008;42(3):254–259.
17. Forbes B, Ehrhardt C. Human respiratory epithelial cell culture for drug delivery applications. *Eur J Pharm Biopharm*. 2005;60(2): 193–205.
18. Yoo JW, Kim YS, Lee SH, et al. Serially passaged human nasal epithelial cell monolayer for in vitro drug transport studies. *Pharm Res*. 2003; 20(10):1690–1696.
19. Liang XL, Zhang J, Zhao GW, et al. Mechanisms of improvement of intestinal transport of baicalin and puerarin by extracts of Radix Angelicae Dahuricae. *Phytother Res*. 2015;29(2):220–227.
20. Tsukita S, Furuse M, Itoh M. Multifunctional strands in tight junctions. *Nat Rev Mol Cell Biol*. 2001;2(4):285–293.
21. Van Itallie CM, Anderson JM. Architecture of tight junctions and principles of molecular composition. *Semin Cell Dev Biol*. 2014;36: 157–165.
22. Runkle EA, Mu D. Tight junction proteins: from barrier to tumorigenesis. *Cancer Lett*. 2013;337(1):41–48.
23. Velarde G, Ait-Aissa S, Gillet C, et al. Use of transepithelial electrical resistance in the study of pentachlorophenol toxicity. *Toxicol In Vitro*. 1999;13(4–5):723–727.

24. Hirsch M, Noske W. The tight junction: structure and function. *Micron*. 1993;24(3):325–352.
25. Turner JR, Buschmann MM, Romero-Calvo I, Sailer A, Shen L. The role of molecular remodeling in differential regulation of tight junction permeability. *Semin Cell Dev Biol*. 2014;36:204–212.
26. Stromskaya TP, Rybalkina EY, Zabotina TN, Shishkin AA, Stavrovskaya AA. Influence of RAR α gene on MDR1 expression and P-glycoprotein function in human leukemic cells. *Cancer Cell Int*. 2005; 5(1):1–9.
27. Liu L, Zhao X, Zhu D, Cheng YY, Qu HB. Simultaneous LC-MS/MS determination of danshensu and paeoniflorin for permeability studies in Caco-2 intestinal absorption model. *Chem Res Chinese Univ*. 2008; 24(4):420–426.
28. Le Grimellec C, Friedlander G, el Yandouzi EH, Zlatkine P, Giocondi MC. Membrane fluidity and transport properties in epithelia. *Kidney Int*. 1992;42(4):825–836.